Clays and Clay Minerals, Vol. 61, No. 6, 499–507, 2013.

SPIRAL STRUCTURE OF 7 Å HALLOYSITE: MATHEMATICAL MODELS

GIRIJA BHUSHAN MITRA*,†

Indian Association for the Cultivation of Science, Jadavpur, Calcutta 700 032, West Bengal, India

Abstract—Halloysite is used for targeted delivery of drugs and other biomolecules. Renewed interest in examination by X-ray diffraction (XRD) to predict the size of particles that can be loaded onto the nanotubes has resulted. Anhydrous halloysite consists of spiraled tubules the length and diameter of which can be determined by measurement using an electron microscope. In spite of ample evidence regarding the spiral structure of halloysite, current programs to evaluate the structure of halloysite nanotubes consider it to be a hollow tube or a cylinder which prevents accurate prediction of its structure and leads to misinformation about the sizes of materials that can be loaded onto the nanotubes. The overall objective of the current study was to derive equations to estimate the structure of halloysite nanotubes which take into consideration its spiral structure. The study of Fourier transform either by electron diffraction or XRD led to the measurement of the spiral thickness and the nature of the spiral. Calculations of the nanotube dimensions may determine the ability of these carriers to allow the mechanical delivery of certain drugs. Here the structure of hydrated halloysite (hollow cylindrical tubes with a doughnut-like cross-section) and anhydrous halloysite (spiraled or helical structure) are described as previously reported in the literature. The Fourier transform of the spiraled structure was selected based on three different kinds of spirals: the Archimedean spiral, the Power spiral, and the Logarithmic spiral. Programs used to define the crystal structure of materials and to calculate the Fourier transform need to take the spiral structure into consideration.

Key Words—Archimedean Spirals, Electron Microscopy, Fourier transform, Halloysite Nanotubes, Logarithmic Spirals, Power Spirals, X-ray Diffraction.

INTRODUCTION

Halloysite is a two-layered 1:1 aluminosilicate clay mineral first identified in 1826: it is a member of the kaolinite group of minerals which includes kaolinite, dickite, nacrite, and halloysite, all of which have the same chemical composition but different crystal structures. Of these, dickite has the greatest structural order, and halloysite, the least; but their atomic arrangements are similar. In fact, some early investigators used the structure factors of dickite to represent the structure factors of halloysite (Cowley, 1961); the main difference between the kaolin-group minerals is the layer stacking sequence.

Halloysite nanotubes have been used in ceramics, cements, and fertilizers, and have recently been used as bionanomaterials, and in biocomposite films. Because of its biocompatibility, halloysite has potential application in biopolymer composites, in bone implants, in controlled delivery of drugs and other biomolecules to selected target organ sites, and as an anti-corrosive agent, *etc*. (Levis and Deasy, 2002, 2003; Shchukin *et al.*, 2005; Lvov *et al.*, 2008; Abdullayev *et al.*, 2009; Viseras *et al.*, 2009; Shi *et al.*, 2011; Brondani *et al.*, 2012; Ghebaur *et al.*, 2012; Qi *et al.*, 2012; Qiao *et al.*, 2012; Vergaro *et al.*, 2012). Because of their structure, halloysite nanotubes have recently even been proposed as filters for the capture of circulating tumor cells (Hughes and King, 2010). The mineral is attractive because of its low toxicity, easy uptake, and low cost (Vergaro *et al.*, 2010).

Hydrated halloysite has been shown to have a tubular or tube-like structure, depending on whether the material had been subjected to surface tension or not (Hope and Kittrick, 1964; Kohyama *et al.*, 1978). This mineral commonly exists in two forms – the space between the inner and outer layers of Al hydroxide corresponding to stacked layers at intervals of ~7.2–7.5 Å in dehydrated halloysite and 10 Å in hydrated halloysite. Previous studies have derived the following structure of dehydrated (7 Å) halloysite (Mitra and Bhattacherjee, 1975): a = 7.6 Å, b = 8.90 Å, c = 5.14 Å, β = 96º45′, where the a and b axes of the unit cells are along the circumference of the cylinder, while the c axis is parallel to the long axis of the cylinder. The comparatively large radius of the cylinder will cause little change in the magnitudes of the a and b values. In contrast, the selected area electron diffraction pattern showed the dimensions of hydrated (10 Å) halloysite as two-layer periodicity in a monoclinic structure with unit-cell parameters of a = 5.14 (10.28) Å, b = 8.90 Å, c = 20.7 Å, β = 99.7º in space group *Cc* (Kohyama *et al.*, 1978).

* E-mail address of corresponding author:
gbmitra@gmail.com
† Current Address: 284B Rash Behari Avenue, Kolkata – 700 019, West Bengal, India
DOI: 10.1346/CCMN.2013.0610602

Incidentally, *a* and *b* are not straight lines; they are curved (Mitra and Bhattacherjee, 1975). Such curvature had already been observed in the unit cells of kaolinite, the representative mineral of the kaolin group (Mitra, 1957). In 1977, spiraling was proposed as a possible structure for halloysite (Kirkman, 1977), and later this was validated by experimental observation, suggesting that growth of halloysite into curved surfaces may be due to a continuous distribution of crystal dislocations (Kirkman, 1981). Transmission electron microscopy (TEM) studies confirmed that kaolinite morphed to halloysite, and that the altered clay first curled into loosely wound spirals; later, the linear parts of the spiral lost their rigidity and became circular or oval in shape (Robertson and Eggleton, 1991). Those authors also proposed that halloysite spirals formed most readily if they had space in which to curl; if space was not available, the halloysite formed sheaves. Recently, high-resolution TEM (HRTEM) showed that dehydrated halloysite is made up of helically rolled parallel cylinders containing spiral cell structures, whereas hydrated halloysite has a more doughnut-like structure (Ece and Schroeder, 2007). On the other hand, even the earliest use of electron microscopy in the study of kaolinite showed that its structure was flaky with less extension in the *c* direction than in the *a* and *b* directions (Mitra, 1963). Thus, 7 Å halloysite is analogous to a disordered kaolinite structure.

Despite the initial observation of a spiral structure, more recent analyses of the crystal structure of halloysite have ignored the spiral configuration (Zhang *et al.*, 2012). The present author has derived relationships for various deformities in crystal structure, deriving the Fourier transform for these forms in terms of spirals with varying radii (Mitra, 2012). Three types of spirals were considered, namely: (1) Archimedean spiral; (2) involute of a circle or Power spiral; and (3) Logarithmic spiral, as defined by Vigodsky (1975). Spiraling caused the radius r to be modified by a factor $f(\theta)$, so that r becomes $rf(\theta)$ (Mitra, 2012), where $f(\theta) = \theta$ for Archimedean helix, θ^n for Power helices such as $\theta^{1/2}$ for Fermat's helix, θ^{-1} for hyperbolic helix, and e^{θ} or $e^{-\theta}$ for the Logarithmic helix (as defined by Ferris *et al.*, 2001), r and θ being co-ordinates of the map on which the helix is drawn, such that $f(\theta)$ is unaffected by the magnitude of r.

The structure of halloysite had been partially explained in terms of an Archimedean spiral (Bursill, 1990); however, not all spiral structures can be explained in terms of the Archimedean spiral, and other forms of spirals may be better suited to explain the crystal structure of the various forms of halloysite nanotubes that have varying inner and outer diameters. In the present study, the author explains the spiral structure of 7 Å halloysite using not only an Archimedean spiral but also a Power spiral, and a Logarithmic spiral.

METHODOLOGY

Representation of a spiral lattice

An equation is derived here to explain the XRD structure of halloysite nanotubes in terms of the Fourier transform of a series of atoms placed equiangularly on the arc of a spiral. A spiral has been defined in terms of a circular arc that does not close, due to a change in the radius, in contrast to a circle, which has a constant radius and, therefore, closes. N identical atoms spread equiangularly on the arc of a circle of a radius r (Figure 1), if irradiated by a parallel beam of electromagnetic rays of wavelength λ, has been assumed to form a lattice given by

$x_j = r \cos \theta_j$ and
$y_j = r \sin \theta_j$ where j is the order of the atom in the lattice.

The corresponding reciprocal lattice is given by

$$H = S \cos \varphi \text{ and}$$
$$K = S \sin \varphi$$

where S is the space between two atoms and φ is the corresponding angle in reciprocal space.

The Fourier transform is given by

$G(s) = \sum(x_j + iy_j)(H - iK) = rSe^{i\theta_j}e^{i\varphi}$ in this case.

Fourier transform for N atoms spaced equiangularly on the arc of a circle

The circle is considered to have a radius r, and the spacing between two consecutive atoms being α,

$$G(s) = \sum_{r=1}^{N-1} \exp\left|-\frac{2\pi i}{\lambda} rS[\cos(r\varphi + \alpha) - \cos(r\varphi + \alpha_0)]\right| \quad (1)$$

$$= \left(\frac{\exp 4\pi i}{\lambda} r \frac{\sin \alpha + \alpha_0}{\lambda} ? \frac{\sin \alpha - \alpha_0}{\lambda}\right)$$
$$\sum \frac{i4\pi s}{\lambda} \sin(r\varphi + \theta + \alpha_0) \sin \theta \quad (2)$$

where $\alpha - \alpha_0 = 2\theta$ and α_0 is a constant.

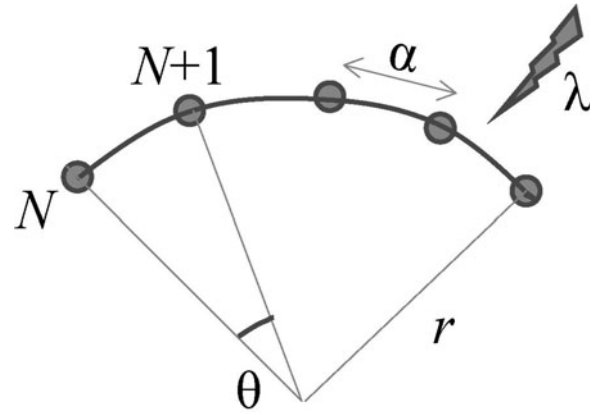

Figure 1. Representation of N identical atoms spread equiangularly on the arc of a circle of a radius r.

https://doi.org/10.1346/CCMN.2013.0610602 Published online by Cambridge University Press

Using the relation

$$\exp(ix\ \sin\theta) = \sum_{p=-\infty}^{\infty} J_p(x)\exp(ip\theta)$$

where $J_p(x)$ is the Bessel function of the first kind of order p and argument x, the following equation may be derived:

$$G(s) = \frac{\exp i4\pi}{\lambda} r\sin(\theta+\alpha_0)\sin\theta \sum_{p=-\infty}^{\infty}\sum_{r=0}^{N-1} J_p\left[\frac{8\pi ir}{\lambda}\sin\theta\right]\exp[ip(r\varphi+\theta+\alpha_0)] \quad (3)$$

Intensity of scattered radiation

The intensity of radiation scattered in the direction

$$F(s) = 2\pi\int_{r_2}^{r_1} J_0(2\pi rS)rdr = \frac{r_1J_1(2\pi r_1S) - r_2J_2(2\pi r_2S)}{S}$$

is given by

$$I(\theta) = f^2(\theta)N^2J_0^2\left(\frac{4\pi}{\lambda}r\sin\theta\right)2f^2\theta \sum_{p=-\infty}^{\infty} J_p\left(\frac{4\pi r}{\lambda}\sin\theta\right)\frac{\sin^2 Np\frac{\varphi}{2}}{\sin^2 p\frac{\varphi}{2}} \quad (4)$$

When the arc contains N atoms, for a full circle:

$$N = (2\pi r/\alpha) \text{ and}$$

$$I(\theta) = f^2(\theta)\frac{4\pi^2r^2}{\alpha^2}J_0^2\left(\frac{4\pi}{\lambda}r\sin\theta\right) + 2f^2\theta \sum_{p=-\infty}^{\infty} J_p\left(\frac{4\pi}{\lambda}r\sin\theta\right)\frac{\sin^2\frac{2\pi r}{\lambda}p\frac{\varphi}{2}}{\sin^2 p\frac{\varphi}{2}} \quad (5)$$

With p as an integer, $J_{-p}(x) = (-1)^pJ_p(x)$, and so the odd values of p cancel each other out and, therefore, equation 5 can be written as

$$I(\theta) = f^2(\theta)\frac{4\pi^2r^2}{\alpha^2}J_0^2\left(\frac{4\pi}{\lambda}r\sin\theta\right) + 2f^2\theta \sum_{p=-\infty}^{\infty} J_p\left(\frac{2\pi r}{\lambda}\sin\theta\right)\frac{\sin^2\frac{2\pi r}{\lambda}p\frac{\varphi}{2}}{\sin^2 p\frac{\varphi}{2}} \quad (6)$$

RESULTS FROM APPLICATIONS TO HALLOYSITE

The spiraled nanotubes of halloysite were shown to be long and hollow with the thickness being a measure of the number of turns of the spiral and the distance between individual turns due to each spiral. Hydrated halloysite nanotubes consist of doughnut-shaped structures, which are, in essence, hollow cylinders, whereas the structure of dehydrated halloysite consists of spiraled tubes (Ece and Schroeder, 2007). Various configurations for these spiraled halloysite nanotubes have been proposed (Bursill, 1990), explained in terms of an Archimedean spiral only, but the Fourier transform of these structures was not established. In order to calculate the Fourier transform of a spiraled nanotube, the Fourier transform of a solid rod will first be estimated and then extended to yield the Fourier transform of a hollow cylinder, which may represent the structure of hydrated halloysite as described by Ece and Schroeder (2007). The Fourier transform of the various types of spirals described may then be derived by treating a spiraled rod as a hollow cylinder of varying radii (Figure 2).

Fourier transform of a solid rod of plugged halloysite

Halloysite carrying material through its nano-pores will appear as plugged solid rods. A solid rod can be considered as a series of tubes with varying radii. A solid circular cylinder of radius, r, and constant length, l, has been described elsewhere (Mitra, 2012) by:

$x = r\cos\theta$ and $y = r\sin\theta$ ($z = l$ being constant, does not affect the calculations).

Let the corresponding reciprocal lattice be given by $H = S\cos\varphi$ and $K = S\sin\varphi$. In the case of feldspar rods of constant length, l, which is typically in the range 0.5–2.0 μm (Abdullayev and Lvov, 2010), the equations derived by Mitra (2012) may be modified to yield the Fourier transform of the cylinder as:

$$F(S) = \int_0^r \exp[2\pi irS]\cos(\theta - \varphi)dr \quad (7)$$

A typical mineral rod would consist of flakes of material with layer spacing of ~0.72 nm in the case of a dehydrated halloysite (Abdullayev and Lvov, 2010). Taking each layer as a circular disc:

$$\int_0^r \exp[i(2\pi rS\cos\varphi)]\exp[in\varphi]d\varphi = 2\pi i^nJ_n(2\pi rs) \quad (8)$$

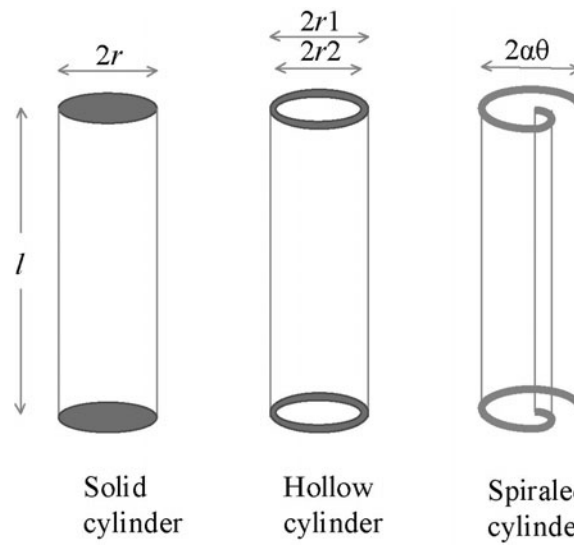

Figure 2. Representation of the halloysite nanotube as a solid cylinder, a hollow cylinder, and a spiraled cylinder.

https://doi.org/10.1346/CCMN.2013.0610602 Published online by Cambridge University Press

where $J_n(x)$ is the Bessel function of order n.

Hence,

$$\int_0^r \exp[i2\pi rS]\cos[\varphi d\varphi] = 2\pi J_0(2\pi rs) \quad (9)$$

Thus,

$$F(S) = \int_0^r \exp[i\{2\pi rS\cos(\theta-\varphi)d\varphi r\}]dr = 2\pi r\int_0^r J_0(2\pi rS)rdr \quad (10)$$

$$\int_0^r J_m(2\pi rS)(2\pi rS)^{m+1}d(2\pi rS) = (2\pi rS)^{m+1}J_{m+1}(2\pi rS) \quad (11)$$

for the Bessel function of order m.

Assuming $m = 0$, which is the special case for solid, cylindrical rod-shaped structures of uniform radius, r, and fixed length, consisting of multi-layered flakes:

$$\int_0^r J_0(2\pi rS)2\pi rSd(2\pi rS) = (2\pi rS)\frac{J_1(2\pi rS)}{S} \quad (12)$$

Fourier transform of a rolled hollow tube of hydrated halloysite

Electron microscopy revealed that the structure of hydrated halloysite typically consists of rolled hollow tubes (Ece and Schroeder, 2007). Let the hollow circular cylinder have external and internal radii r_1 and r_2, respectively. Proceeding as in the previous case, equation 10 for a hollow cylinder can be written as:

$$F(S) = 2\pi\int_{r_2}^{r_1} J_0(2\pi rS)rdr = \frac{r_1J_1(2\pi r_1S) - r_2J_1(2\pi r_2S)}{S} \quad (13)$$

as shown previously (Mitra, 2012).

Extending this equation to calculate the intensity scattered in the direction $S = (2\sin\theta)/\lambda$, the following relationship can be obtained:

$$I(S)s^2 = F^2(s)S^2 = [r_1J_1(2\pi r_1S) - r_2J_1(2\pi r_2S)]^2$$

note that $J_1(x) = \frac{x}{2} - \frac{x^3}{16}$ (Pierce and Foster, 1966 – equation 761)

So that

$$\begin{aligned} SF(s) &= r_1J_1(2\pi r_1S) - r_2J_1(2\pi r_2S) \\ &= r_1\left[\frac{2\pi r_1S}{2} - \frac{8\pi^3r_1^3S^3}{16}\right] - r_2\left[\frac{2\pi r_2S}{2} - \frac{8\pi^3r_2^3S^3}{16}\right] \\ &= \left[\pi r_1^2s - \frac{\pi^3}{2}r_1^4s^3\right] - \left[\pi r_2^2s - \frac{\pi^3}{2}r_2^4s^3\right] \\ &= \pi(r_1^2 - r_2^2)s - \frac{\pi^3s^3}{2}(r_1^4 - r_2^4) \\ &= \pi s(r_1^2 - r_2^2) - \frac{\pi^3s^3}{2}(r_1^4 - r_2^4) \end{aligned}$$

Therefore,

$$\begin{aligned} S^2I(s) &= \pi^2s^2(r_1^2 - r_2^2)^2 + \frac{\pi^6s^6}{4}(r_1^4 - r_2^4)^2 - \\ &\quad 2\pi s(r_1^2 - r_2^2)\frac{\pi^3s^3}{2}(r_1^4 - r_2^4) \\ &= \pi^2s^2(r_1 - r_2)(r_1 + r_2) + \\ &\quad \frac{\pi^6s^6}{4}(r_1 - r_2)(r_1 + r_2)(r_1^2 + r_2^2) - \\ &\quad 2\pi s(r_1 + r_2)(r_1 - r_2)\frac{\pi^2s^6}{2}(r_1 + r_2)(r_1 - r_2)(r_1^2 + r_2^2) \end{aligned}$$

Typically, the size of the inner lumen of a halloysite nanotube is ~15 nm while that of the outer diameter is ~50 nm (Abdullayev and Lvov, 2010). If the inner and outer diameters of the halloysite nanotubes are vastly different, then no other modifications to this equation are necessary.

Calculation of the thickness of a thin-walled hollow halloysite cylinder following internal etching

Selective etching of the inner surface of Al oxide to enlarge the lumen increases the loading capacity of the halloysite nanotube and increases the sustained release of active chemical agents (Abdullayev *et al.*, 2012). When that happens, the thickness of the walls decreases and the thickness of the wall can be interpreted by a slight modification to the above equation(s). If the tube wall is exceedingly thin, r_1 and r_2 are nearly the same, so that

$$\begin{aligned} &r_1^2 - r_2^2 \\ &= (r + t)^2 - r^2 \text{where } t \text{ is the thickness of the wall} \\ &= 2t + t^2 = 2t. \text{ Ignoring } t^2 \text{ (as } t \text{ is very small),} \\ &= \pi^2s^2 2rt + \tfrac{\pi^6s^6}{2}(2r^2)2rt - 2\pi s2rt\tfrac{\pi^2s^2}{2}2r^2 2rt \\ &= 4\pi^2s^2rt(1 - 4\pi sr) \\ I(s) &= 4\pi^2rte^{-4\pi sr} \end{aligned} \quad (14)$$

$$\begin{aligned} \text{Thus, } \ln I(s) &= \ln(4\pi^2rt) - 4\pi sr \\ &= \ln(4\pi^2r) + \ln t - 4\pi sr \\ &= [\ln(4\pi^2r) - 4\pi sr] + \ln t \end{aligned}$$

This equation is now applied to that of a hollow cylinder of hydrated halloysite or kaolinite. If s_1 and s_2 are interatomic distances in two dimensions of the cylinder, taking two values of $I(s)$ at $s = s_1$ and s_2, where s_1 and s_2 may typically be the interatomic distances in the outer silica surface and the inner surface of Al oxide:

$$\ln I(s_1) = [\ln(4\pi^2r) - 4\pi s_1r] + \ln t,$$

and

$$\ln I(s_2) = [\ln(4\pi^2r) - 4\pi s_2r] + \ln t,$$

so that $[\ln I(s_1) - \ln I(s_2)] = 4\pi(s_2 - s_1)r$

and

$$r = \frac{\ln I(s_1) - \ln I(s_2)}{4\pi(s_2 - S_1)} \quad (15)$$

https://doi.org/10.1346/CCMN.2013.0610602 Published online by Cambridge University Press

The thickness of the hollow halloysite cylinder can be obtained by substituting this value of r in equation 14, where:

$$I(s) = \pi t \frac{\ln I(s_1) - \ln I(s_2)}{(s_2 - s_1)} e^{-s\frac{\ln I(s_1) - \ln I(s_2)}{(s_2 - s_1)}} \quad (16)$$

This equation may be applied to studies showing that t = 4.263 Å, s_{inner} = 8.655 Å, and s_{outer} = 9.164 Å (Singh, 1996). Further etching may reduce t to 1.62 Å.

Effect of spiraling on the structure of dehydrated halloysite nanotubes

The structure of dehydrated (anhydrous) halloysite is known to consist of spiraled structures that make up the tubular wall (Abdullayev and Lvov, 2010; Joo *et al.*, 2012). Therefore, the equations derived above will now be extended to that of thin-walled spirals which, in combination, make up the thicker walls of the nanotubes. In contrast to a circle, a spiral will have varying radius, and accordingly, the three types of spirals discussed above (Figure 3) will be:

1. The Archimedean Spiral. As seen in Figure 3, an Archimedean spiral can be represented by a radius: $r = a\theta$, where a is independent of r and θ (θ can be positive or negative). Hence, for such spirals:

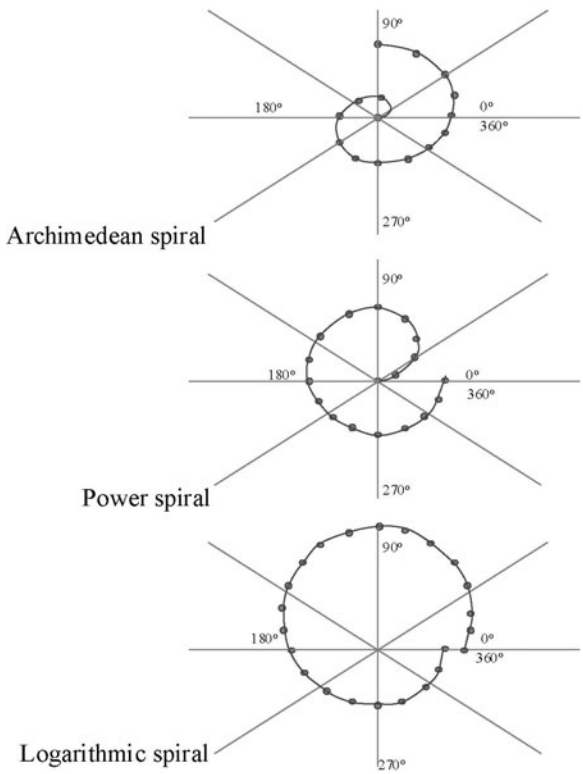

Figure 3. Representation of atoms arranged as an Archimedean spiral, a Power spiral, and a Logarithmic spiral.

$$I(\theta) = f^2(\theta)4\pi^2\theta^2 J_0^2\left(\frac{4\pi}{\lambda}a\theta\sin\theta\right) + 2f^2(\theta)\sum_{p=-\infty}^{\infty} J_p\left[\frac{2\pi a\theta}{\lambda}\sin\theta\right]\frac{\sin^2\frac{2\pi a\theta}{\lambda}p\frac{\varphi}{2}}{\sin^2 p\frac{\varphi}{2}} \quad (17)$$

Therefore, in case of an Archimedean spiral, where $r = a\theta$, equation 14 can be written as:

$$I(s) = 4\pi^2 a\theta t e^{-4\pi s a\theta} \quad (18)$$

However, an Archimedean spiral will basically be equivalent to a solid rod which has already been discussed. For mostly hollow tubes, the structure for a thick-walled tube is better represented by a Power spiral while a thin-walled tube may have a spiral with a wider diameter as represented by a Logarithmic spiral.

2. The Power spiral. In this case, the radius of the spiral will be represented by $r = a\theta^n$, where a and n are constants independent of the polar coordinates r and θ (n may be positive or negative). For a Power spiral, therefore:

$$I(\theta) = f^2(\theta)4\pi^2\theta^{2n} J_0^2\left(\frac{4\pi}{\lambda}a\theta^n\sin\theta\right) + 2f^2(\theta)\sum_{p=-\infty}^{\infty} J_p\left[\frac{2\pi a\theta^n}{\lambda}\sin\theta\right]\frac{\sin^2\frac{2\pi a\theta^n}{\lambda}p\frac{\varphi}{2}}{\sin^2 p\frac{\varphi}{2}} \quad (19)$$

Freeze-fracture HRTEM replicas of dehydrated halloysite from Balikesir, Turkey (Ece and Schroeder, 2007) may be represented by such Power spirals.

For the special case of Fermat's spiral ($r = a\theta^{1/2}$):

$$I(\theta) = f^2(\theta)4\pi^2\theta J_0^2\left(\frac{4\pi}{\lambda}a\theta^{1/2}\sin\theta\right) + 2f^2(\theta)\sum_{p=-\infty}^{\infty} J_p\left[\frac{2\pi a\theta^{1/2}}{\lambda}\sin\theta\right]\frac{\sin^2\frac{2\pi a\theta^{1/2}}{\lambda}p\frac{\varphi}{2}}{\sin^2 p\frac{\varphi}{2}} \quad (20)$$

Whereas for a hyperbolic spiral ($r = a\theta^{-1}$),

$$I(\theta) = f^2(\theta)4\pi^2\theta J_0^2\left(\frac{4\pi a}{\lambda\theta}\sin\theta\right) + 2f^2(\theta)\sum_{p=-\infty}^{\infty} J_p\left[\frac{2\pi a}{\lambda\theta}\sin\theta\right]\frac{\sin^2\frac{2\pi a}{\lambda\theta}p\frac{\varphi}{2}}{\sin^2 p\frac{\varphi}{2}} \quad (21)$$

For these and other Power spirals,

$$I(s) = 4\pi^2 a\theta^n t e^{-4\pi s a\theta^n} \quad (22)$$

3. The Logarithmic spiral. For a thin-walled halloysite nanotube that curls, either naturally or due to disruption of the inner surface caused by chemical or physical strain, the walls will be represented neither by an Archimedean nor by Power spirals. The only spiral that can represent the tube in this case will be a Logarithmic spiral of radius:

https://doi.org/10.1346/CCMN.2013.0610602 Published online by Cambridge University Press

$r = ae^{-\theta}$, where a is constant. Here,

$$I(\theta) = f^2(\theta)4\pi^2 e^{-\theta} J_0^2\left(\frac{4\pi}{\lambda} ae^{-\theta}\sin\theta\right) + 2f^2(\theta)\sum_{p=-\infty}^{\infty} J_p\left[\frac{2\pi ae^{-\theta}}{\lambda}\sin\theta\right]\frac{\sin^2\frac{2\pi ae^{-\theta}}{\lambda}p\frac{\varphi}{2}}{\sin^2 p\frac{\varphi}{2}} \quad (23)$$

Hence for a logarithmic spiral:

$$I(s) = 4\pi^2 a\ \exp[-\theta]t\ \exp[-4\pi sa\ \exp[-\theta]] \quad (24)$$

The Fourier transform of the scattering of radiation from a circular scatterer of radius 2 Å subject to spiraling of an Archimedean spiral, a Power spiral where n = 2, and a Logarithmic spiral is shown in Figure 4.

DISCUSSION

The theory of line broadening due to particle size and strain in XRD patterns to decipher mineral structure was worked out as early as in 1953 (Williamson and Hall, 1953). Instead of line broadening, here, line distortion in the halloysite crystal due to a spiral structure is being considered. In the hydrated state (10 Å halloysite), halloysite is in the form of a doughnut-shaped cross-section (Ece and Schroeder, 2007), which implies that the hydrated halloysite nanotube will consist of a hollow cylindrical rod, whereas anhydrous halloysites have a spiral structure. Initial reports (Waser, 1955) showed that halloysite nanotubes were ~3000 Å long and 300 Å in radius; later studies also reported halloysite nanotubes to be ~1000 Å in diameter (Cowley, 1961). Halloysite nanotubes have now been established to be of 15−100 nm inner diameter, and up to 500−1000 nm long (Lvov *et al.*, 2008). The structure of halloysite closely resembles that of kaolinite and often it is difficult to distinguish between the two − this is to be expected because kaolinite and halloysite are common products of weathering and hydrothermal alterations in feldspar (Tazaki and Fyfe, 1987). Studies have provided explanations for the mechanism by which planar kaolinite rolls to tubular halloysite (Singh, 1996). Powder XRD patterns of the two minerals overlap and can be transformed from one to the other (La Iglesia and Galán, 1975; Bobos *et al.*, 2001; Oliveira *et al.*, 2007).

The banded character of many of the XRD lines from halloysite has been attributed to its structure being equivalent to a random stacking of two-dimensional silicate sheets. Initial studies (Warren, 1941) established the theory of random stacking of two-dimensional layers. Halloysite was shown to consist of layers that were arranged parallel and equidistant but random in translations parallel to the layer and in rotation about the normal. Analysis of the structure of dehydrated halloysite on the basis of this distorted structure (Brindley and Robinson, 1948) showed that X-ray reflections of halloysite could be grouped into two categories: (1) the basal 00l reflections, which can be considered as the

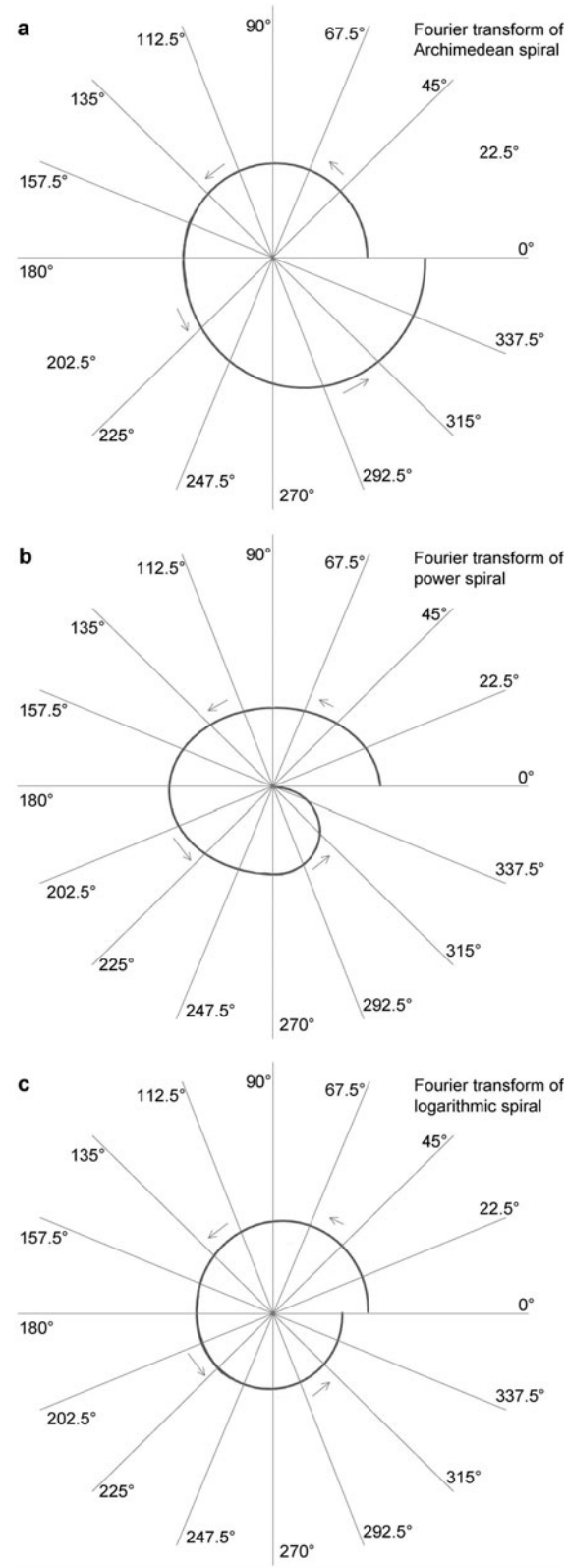

Figure 4. Fourier transform of the scattering of radiation from a circular scatterer of radius 2 Å subject to spiraling of the three types.

https://doi.org/10.1346/CCMN.2013.0610602 Published online by Cambridge University Press

only three-dimensional reflections; and (2) two-dimensional *hk* bands.

Minerals such as chrysotile and halloysite show additional cylindrical structures with spirals (Jagodzinski and Kunze, 1954a, 1954b, 1954c; Taggart *et al.*, 1954). Observation of small fragments of halloysite by electron microscopy found that they were wrapped in spirals that formed tubular stacks (Honzo and Mihama, 1954). These stacks were formed by bending and twisting three-dimensional crystallites into curvaceous shapes (Waser, 1955; Singh, 1996), and the spirals were in the form of involutes of circles (Whittaker, 1955). Multiple studies have concentrated on the formation of the spiraled structure of dehydrated halloysite from a cylindrical hydrated structure, mainly the transformation of kaolinite to halloysite (Kirkman, 1981; Robertson and Eggleton, 1991; Bobos *et al.*, 2001). In chrysotile and other minerals such as cylindrite a structure that consists of two interleaved spirals was initially proposed (Whittaker, 1956). Later studies (Bursill, 1990) showed that structures consisting of these interleaved spirals can result in a configuration that would ultimately result in a solid cylinder-like pattern. Equation 14 can distinguish between these two patterns by measuring the thickness t; therefore, this equation can have wide efficacy beyond the measurement of the simple spiral configuration.

Only two-dimensional spirals have been described thus far. Jagodzinski and Kunze (1954b) described two types of basic spiral configurations: the simple cylindrical helix, which considers a spiral in the two-dimensional plane, and as a simple Archimedean spiral where the crystal growth is in the form of a three-dimensional spiral (Jagodzinski and Kunze, 1954c). Unlike that which has been derived in the present work, which considered the two-dimensional case selectively, in the three-dimensional spiral, z will not be constant but will also be a function of the angle θ. In that case, equation 14 will have to be extended taking the z axis into consideration.

The implications of this work need to be explained in terms of the utility of halloysite nanotubes in biopolymers. Halloysite obtained from New Zealand was shown by electron microscopy to be typically 2−3 μm long, to have outer and inner diameters of 0.3 and 0.1 μm, respectively, and to consist of aggregates of hollow microtubules, double tubules, and split of partially unrolled tubules (Levis and Deasy, 2002). Significantly, smaller molecules such as glycerol can be exchanged easily on these tubes whereas larger molecules such as diltiazem HCl failed to exchange (Levis and Deasy, 2002). On the other hand, the less water-soluble propranol HCl showed greater sustained release effect, and even diltiazem HCl showed greater efficacy when the tubules were treated with polyethyleneimine (Levis and Deasy, 2003), and diphenhydramine HCl was shown to undergo slow drug release from halloysite nanotubes coated with biodegradable polymer (Ghebaur *et al.*, 2012). The anti-inflammatory drug 5-aminosalycilic acid (5-ASA) could also be loaded onto nanotubes with approximate dimensions of 0.1 μm (Viseras *et al.*, 2009). Resveratrol, a polyphenol known for having antioxidant and antineoplastic properties, could also be loaded into halloysite nanotubes for sustained release to breast-cancer cells using halloysite nanotubes (Vergaro *et al.*, 2012). These results showed that the structure and physical dimensions of the halloysite nanotube dictates the limitation and delivery of the items that the nanotube can carry.

Drugs are not the only compounds that halloysite nanotubes can carry. The corrosion inhibitor benzotriazole was loaded up to 5% onto nanotubes of 50 nm external diameter and a lumen of 15 nm (Abdullayev *et al.*, 2009). Halloysite nanotubues can be used as gene-delivery agents (Shi *et al.*, 2011) and in the development of a new biosensor for the determination of catecholamines by square-wave voltammetry (Brondani *et al.*, 2012). Halloysite nanotubes were used for doping in the construction of organic/inorganic nanofiber systems (Qi *et al.*, 2012), and to prevent the cracking of polymer latex films (Qiao *et al.*, 2012). All these mechanical properties of the nanotube also depend on the overall dimensions of the individual nanotubes.

The world's halloysite nanotubes are all of different is dimensions. In addition, the surface chemistry of halloysite nanotubes is readily modified (Yuan *et al.*, 2008) especially chemically, such as with organosilanes (Yuan *et al.*, 2012a) or with physical effects such as heating (Yuan *et al.*, 2012b). These modifications also cause alterations in the structure of the nanotubes and therefore the potential use of the tube. Halloysite has a number of hydroxyl groups on its surface. The external morphology of halloysite nanotubes consists of siloxane groups (Si−O−Si); at the same time, other groups (such as hydroxyl group, Al−OH) line the internal surface of the nanotubes (Joo *et al.*, 2012). Modification of the functional groups altered the carrier properties of the halloysite nanotubes (Joo *et al.*, 2012); however, the coating of the nanotubes by the biopolymers, and other compounds will also alter the inner diameter and the dimensions of the nanotube. This may affect the drug-/ion-carrying capacity; therefore, one can identify the dimensions of the nanotube before embarking on the loading of a new compound. The current study provides the tools for determining these dimensions.

CONCLUSIONS

The Fourier transform equation for a spiral structure of natural dehydrated halloysite has been established and can be incorporated into computer programs that specifically target interpretations of such structures. The main equation to be used for such an interpretation is #14, which is equivalent to a Williamson and Hall

https://doi.org/10.1346/CCMN.2013.0610602 Published online by Cambridge University Press

equation for a hollow cylindrical rod with $4\pi r^2 t$ being the apparent particle size and $4\pi sr$ the apparent strain, while the size and strain can be refined further using the second and fourth moment calculations included here in equations 13 and 15. Using these equations, existing computer programs can be modified easily to measure the radius and thickness of the hollow cylinder structure of halloysite.

ACKNOWLEDGMENTS

The author is indebted to Dr Paramita M. Ghosh, University of California at Davis, California, USA for assistance with the language in this manuscript. He is also indebted to Shri Bishwajit Halder for secretarial help.

REFERENCES

Abdullayev, E. and Lvov, Y. (2010) Clay nanotubes for corrosion inhibitor encapsulation: Release control with end stoppers. *Journal of Materials Chemistry*, **20**, 6681–6687.

Abdullayev, E., Price, R., Shchukin, D., and Lvov, Y. (2009) Halloysite tubes as nanocontainers for anticorrosion coating with benzotriazole. *ACS Applied Materials and Interfaces*, **1**, 1437–1443.

Abdullayev, E., Joshi, A., Wei, W., Zhao, Y., and Lvov, Y. (2012) Enlargement of halloysite clay nanotube lumen by selective etching of aluminum oxide. *ACS Nano*, **6**, 7216–7226.

Bobos, I.I., Duplay, J., Rocha, J., and Gomes, C.S.F. (2001) Kaolinite to halloysite-7 Å transformation in the kaolin deposit of São Vicente de Pereira, Portugal. *Clays and Clay Minerals*, **49**, 596–607.

Brindley, G.W. and Robinson, K. (1948) X-ray studies of halloysite and metahalloysite. Part I. The structure of metahalloysite, an example of a random layer lattice. *Mineralogical Magazine*, **28**, 393–406.

Brondani, D., Scheeren, C.W., Dupont, J., and Vieira, I.C. (2012) Halloysite clay nanotubes and platinum nanoparticles dispersed in ionic liquid applied in the development of a catecholamine biosensor. *Analyst*, **137**, 3732–3739.

Bursill, L.A. (1990) Quasicrystallography on the spiral of archimedes. *International Journal of Modern Physics B*, **4**, 2197–2216.

Cowley, J. (1961) Diffraction intensities from bent crystals. *Acta Crystallographica*, **14**, 920–927.

Ece, Ö.I. and Schroeder, P.A. (2007) Clay mineralogy and chemistry of halloysite and alunite deposits in the Turplu area, Balikesir, Turkey. *Clays and Clay Minerals*, **55**, 18–35.

Ferris, T.L.J., Nafalski, A., and Saghafifar, M. (2001) Matching observed spiral form curves to equations of spirals in 2-d images. Pp. 151–158 in: *Applied Electromagnetics and Computational Technology* 11 (H. Tsuboi, and I. Sebestyen, editors). IOS Press, Amsterdam.

Ghebaur, A., Garea, S.A., and Iovu, H. (2012) New polymer-halloysite hybrid materials – a potential controlled drug release system. *International Journal of Pharmacy*, **436**, 568–573.

Honzo, G. and Mihama, K. (1954) A study of clay minerals by electron-diffraction diagrams due to individual crystallites. *Acta Crystallographica*, **7**, 511–513.

Hope, E.W. and Kittrick, J.A. (1964) Surface tension and the morphology of halloysite. *American Mineralogist*, **49**, 859–866.

Hughes, A.D. and King, M.R. (2010) Use of naturally occurring halloysite nanotubes for enhanced capture of flowing cells. *Langmuir*, **26**, 12155–12164.

Jagodzinski, H. and Kunze, G. (1954a) Die Rollchenstruktur des Chrysotils. I. Allgemeine Beugungtheorie und Kleinwinkelstreung. *Neues Jahrbuch für Mineralogie Monatshefte*, 95–108.

Jagodzinski, H. and Kunze, G. (1954b) Die Rollchenstruktur des Chrysotils lll. Versetzungswachstum der Rollchen. *Neues Jahrbuch für Mineralogie Monatshefte*, 137–150.

Jagodzinski, H. and Kunze, G. (1954c) Die Rollchenstruktur des Chrysotils. II. Weitwinkleninteferenzen. *Neues Jahrbuch für Mineralogie Monatshefte*, 113–130.

Joo, Y., Jeon, Y., Lee, S.U., Sim, J.H., Ryu, J., Lee, S., Lee, H., and Sohn, D. (2012) Aggregation and stabilization of carboxylic acid functionalized halloysite nanotubes (HNT-COOH). *The Journal of Physical Chemistry C*, **116**, 18230–18235.

Kirkman, J.H. (1977) Possible structure of halloysite disks and cylinders observed in some New Zealand rhyolitic tephras. *Clay Minerals*, **12**, 199–216.

Kirkman, J.H. (1981) Morphology and structure of halloysite in New Zealand tephras. *Clays and Clay Minerals*, **29**, 1–9.

Kohyama, N., Fukushima, K., and Fukami, A. (1978) Observation of the hydrated form of tubular halloysite by an electron microscope equipped with an environmental cell. *Clays and Clay Minerals*, **26**, 25–40.

La Iglesia, A. and Galán, E. (1975) Halloysite-kaolinite transformation at room temperature. *Clays and Clay Minerals*, **23**, 109–113.

Levis, S.R. and Deasy, P.B. (2002) Characterisation of halloysite for use as a microtubular drug delivery system. *International Journal of Pharmacy*, **243**, 125–134.

Levis, S.R. and Deasy, P.B. (2003) Use of coated microtubular halloysite for the sustained release of diltiazem hydrochloride and propranolol hydrochloride. *International Journal of Pharmacy*, **253**, 145–157.

Lvov, Y.M., Shchukin, D.G., Mohwald, H., and Price, R.R. (2008) Halloysite clay nanotubes for controlled release of protective agents. *ACS Nano*, **2**, 814–820.

Mitra, G.B. (1957) X-ray diffraction study of the heat treatment of kaolinite. *Indian Journal of Physics*, **31**, 324–328.

Mitra, G.B. (1963) Structure defects in kaolinite. *Zeitschrift für Kristallographie*, **119**, 161–175.

Mitra, G.B. (2012) Fourier transform of tubular objects with spiral structures. *Journal of Crystallization Process and Technology*, **2**, 133–138.

Mitra, G.B. and Bhattacherjee, S. (1975) The structure of halloysite. *Acta Crystallographica Section B*, **31**, 2851–2857.

Oliveira, M.T.G.d., Furtado, S.M.A., Formoso, M.L.L., Eggleton, R.A., and Dani, N. (2007) Coexistence of halloysite and kaolinite: A study on the genesis of kaolin clays of Campo Alegre basin, Santa Catarina State, Brazil. *Anais da Academia Brasileira de Ciências*, **79**, 665–681.

Pierce, B.O. and Foster, R.M. (1966) *A Short Table of Integrals*, 4th edition. Blaisdell Publishing Co, a Division of Ginn & Co, New York, 96 pp.

Qi, R., Cao, X., Shen, M., Guo, R., Yu, J., and Shi, X. (2012) Biocompatibility of electrospun halloysite nanotube-doped poly(lactic-co-glycolic acid) composite nanofibers. *Journal of Biomaterials Science, Polymer Edition*, **23**, 299–313.

Qiao, J., Adams, J., and Johannsmann, D. (2012) Addition of halloysite nanotubes prevents cracking in drying latex films. *Langmuir*, **28**, 8674–8680.

Robertson, I.D.M. and Eggleton, R.A. (1991) Weathering of granitic muscovite to kaolinite and halloysite and of plagioclase-derived kaolinite to halloysite. *Clays and Clay Minerals*, **39**, 113–126.

Shchukin, D.G., Sukhorukov, G.B., Price, R.R., and Lvov,

Y.M. (2005) Halloysite nanotubes as biomimetic nanoreactors. *Small*, **1**, 510–513.
Shi, Y.F., Tian, Z., Zhang, Y., Shen, H.B., and Jia, N.Q. (2011) Functionalized halloysite nanotube-based carrier for intracellular delivery of antisense oligonucleotides. *Nanoscale Research Letters*, **6**, 608.
Singh, B. (1996) Why does halloysite roll? – a new model. *Clays and Clay Minerals*, **44**, 191–196.
Taggart, M.S., Jr., Milligan, W.O., and Studer, H.P. (1954) Electron micrographic studies of clays. *Clays and Clay Minerals*, **3**, 31–95.
Tazaki, K. and Fyfe, W.S. (1987) Primitive clay precursors formed on feldspar. *Canadian Journal of Earth Sciences*, **24**, 506–527.
Vergaro, V., Abdullayev, E., Lvov, Y.M., Zeitoun, A., Cingolani, R., Rinaldi, R., and Leporatti, S. (2010) Cytocompatibility and uptake of halloysite clay nanotubes. *Biomacromolecules*, **11**, 820–826.
Vergaro, V., Lvov, Y.M., and Leporatti, S. (2012) Halloysite clay nanotubes for resveratrol delivery to cancer cells. *Macromolecular Bioscience*, **12**, 1265–1271.
Vigodsky, M. (1975) *Mathematical Handbook – Higher Mathematics*. Mir Publishers, Moscow.
Viseras, M.T., Aguzzi, C., Cerezo, P., Cultrone, G., and Viseras, C. (2009) Supramolecular structure of 5-aminosalycilic acid/halloysite composites. *Journal of Microencapsulation*, **26**, 279–286.
Warren, B.E. (1941) X-ray diffraction in random layer lattices. *Physical Review*, **59**, 693–698.
Waser, J. (1955) Fourier transforms and scattering intensities of tubular objects. *Acta Crystallographica*, **8**, 142–150.
Whittaker, E. (1955) A classification of cylindrical lattices. *Acta Crystallographica*, **8**, 571–574.
Whittaker, E. (1956) The structure of chrysotile. II. Clinochrysotile. *Acta Crystallographica*, **9**, 855–862.
Williamson, G.K. and Hall, W.H. (1953) X-ray line broadening from filed aluminium and wolfram. *Acta Metallurgica*, **1**, 22–31.
Yuan, P., Southon, P.D., Liu, Z., Green, M.E.R., Hook, J.M., Antill, S.J., and Kepert, C.J. (2008) Functionalization of halloysite clay nanotubes by grafting with γ-aminopropyltriethoxysilane. *Journal of Physical Chemistry C*, **112**, 15742–15751.
Yuan, P., Southon, P.D., Liu, Z., and Kepert, C.J. (2012a) Organosilane functionalization of halloysite nanotubes for enhanced loading and controlled release. *Nanotechnology*, **23**, 375705–375709.
Yuan, P., Tan, D., Annabi-Bergaya, F., Yan, W., Fan, M., Liu, D., and He, H. (2012b) Changes in structure, morphology, porosity, and surface activity of mesoporous halloysite nanotubes under heating. *Clays and Clay Minerals*, **60**, 561–573.
Zhang, H., Lei, X., Yan, C., Wang, H., Xiao, G., Hao, J., Wang, D., and Qiu, X. (2012) Analysis of the crystal structure of 7 Å-halloysite. *Advanced Materials Research*, **415–417**, 2206–2214.

(*Received 1 December 2012; revised 31 October 2013; AE: H. He; Ms. 732*)